Available online at www.sciencedirect.com
ScienceDirect
Scripta Materialia 59 (2008) 1139–1142
Scripta MATERIALIA
www.elsevier.com/locate/scriptamat

Rate-dependent behavior of hierarchical Al matrix composites

H. Zhang,[a,*,1] J. Ye,[b] S.P. Joshi,[a] J.M. Schoenung,[b] E.S.C. Chin[c] and K.T. Ramesh[a]

[a]*Department of Mechanical Engineering, The Johns Hopkins University, Baltimore, MD 21218, USA*
[b]*Department of Chemical Engineering and Material Science, University of California, Davis, CA 95616, USA*
[c]*Army Research Laboratory, Weapons and Materials Research Directorate, Aberdeen Proving Ground, MD 21005, USA*

Received 26 May 2008; accepted 25 July 2008
Available online 3 August 2008

We present the rate-dependent constitutive response of hierarchical Al matrix composites which comprise a bi-modal distribution of Al in fine (nanocrystalline Al containing micro-sized B_4C particles) and coarse (micro-grained Al) grain regimes. The strength of these composites is improved by various strengthening mechanisms. Shear localization is observed to be the primary failure mode. Compared to quaistatic loading, significant increase of strain to failure is observed at high strain rates. Varying rate-sensitivity is observed with different amount of B_4C particles.

Keywords: Hierarchical microstructure; Length-scale effects; Rate-dependent behavior; Metal matrix composite; Strain-to-failure

Particulate-reinforced metal matrix composites (PMMCs) have been identified as attractive materials for numerous applications due to their excellent mechanical and physical properties, ease of manufacture, and low cost of production. One particular application is to work as armors or protective coatings in military or aerospace structures where the materials are often subject to explosive blast loading and dynamic impact. In these applications, understanding the rate-dependent high-strain-rate behavior of PMMCs is important.

A conventional PMMC usually contains two-phases: hard ceramic particles as the reinforcement and a ductile metal as the matrix. The reinforcement particles provide high stiffness and strength to the composite and the metal matrix provides a compliant support for the reinforcement. The strength of PMMCs can be improved by increasing the volume fraction of the reinforcement particles. However, damage such as particle cracking or debonding of particle/matrix interface [1] is usually associated with deformation, and impairs the mechanical properties of PMMCs. As a result, a practical limit of the reinforcement volume fraction exists in fabricating PMMCs. Another approach to improve the strength of PMMCs is to increase the strength of the matrix. Various methods have been used and possibly the most common one is to decrease the grain size [2]. In this material strengthening mechanism the increased volume of grain boundaries act as obstacles to dislocation glide. However, increase in strength of materials with decreased grain size is usually accompanied by a sacrifice of ductility, which limits the use of this approach [3–5]. Recently, it is found by creating a bi-modal structure of nanoscale grains and microscale grains, the ductility in nanocrystalline metals can be significantly increased [6–8].

In this paper, we investigated the compressive constitutive response and failure of three tri-modal composites (composed of micron-grain-sized (MG) Al, nanocrystalline (NC) Al, and micron-sized B_4C particles) at both quasistatic and dynamic strain rates. In dynamic loading, high-speed photography is used to reveal the dynamic failure of these tri-modal composites. This work is an extension to high strain rates of our findings on the super-high strength of similar tri-modal composites under quasistatic loading [9].

These tri-modal composites were produced from a two-step powder mixing (cryomilling and subsequent blending) and hot extrusion process [9] and are designated TM5-20, TM5-45, and TM10-40 (the naming convention is TM-weight%B_4C-weight%NC-Al). Figure 1 presents micrographs showing the overall microstructures of these composites in both extrusion and transverse directions. In these micrographs, the white regions are MG Al particles; the gray regions are NC Al with black B_4C particles distributed in it. The micrographs in Figure 1 indicate uniform microstructures of these tri-modal composites. TEM investigation,

* Corresponding author. Tel.: +1 512 471 4178; e-mail: htzhang@mail.utexas.edu
[1] Present address: Center for Mechanics of Solids, Structures and Materials, The University of Texas, Austin, TX 78712, USA.

1359-6462/$ - see front matter © 2008 Acta Materialia Inc. Published by Elsevier Ltd. All rights reserved.
doi:10.1016/j.scriptamat.2008.07.036

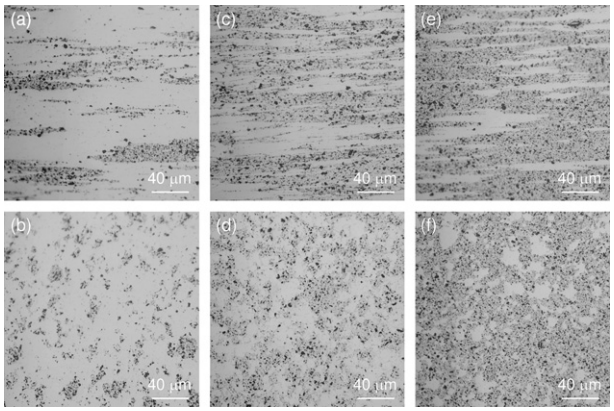

Figure 1. Optical micrographs of: TM5-20 in (a) extrusion direction and (b) transverse direction; TM5-45 in (c) extrusion direction and (d) transverse direction; and TM10-40 in (e) extrusion direction, and (f) transverse direction.

reported elsewhere [9], revealed a clean interface between B_4C particles and NC Al, and high temperature phases were not detected in the interface. The microstructures shown in Figure 1 impart an inherent anisotropy of properties to these composites. In the following text, all of the material properties are those measured along the extrusion direction.

Quasistatic compression tests were performed on a servo-hydraulic MTS machine. Transducer signals of load were obtained using a load cell and the cross-head displacement was measured using a linear variable differential transformer system. Strains were computed from the cross-head displacement after correcting for machine compliance. True stress–strain curves are obtained over a strain rate range of 10^{-4}–10^{-2} s^{-1}. Cylindrical specimens with diameter of 5 mm and length-to-diameter ratio of 2 were cut using a wire EDM. The specimens were lapped with a precision lapping fixture to obtain parallel end surfaces (<5 μm over the diameter). In the test setup, interfaces between the specimen and the compression platens were lubricated with a mixture of grease and solid MoS_2 powder in order to reduce friction.

The compression Kolsky bar (or split-Hopkinson pressure bar) [10] was used to obtain the high strain rate compressive response of the materials over a strain rate range of 10^3–10^4 s^{-1}. The specimens were 5 mm in diameter and 0.6 in length-to-diameter ratio in accordance with standard practice for metallic specimens in Kolsky bar technique. The interfaces between the specimen and bars are adequately lubricated as in quasistatic tests. A digital high-speed camera (DRS Hadland Ultra 8) capable of recording eight frames at 10^8 frames per second was synchronized with the Kolsky bar system to record the deformation and failure of the specimens under dynamic loading. Rectangular specimens ($4 \times 4 \times 2.75$ mm, square cross-section), with one peripheral surface polished to mirror finish, were used in tests with the high-speed camera.

Figure 2a presents the compressive true stress–strain curves of these tri-modal composites under quasistatic strain rates of 10^{-4}–10^{-2} s^{-1}. The true stress–strain curve of the conventional 5083-Al (MG-Al5083, H131 work hardened) [11] is also given for comparison. A

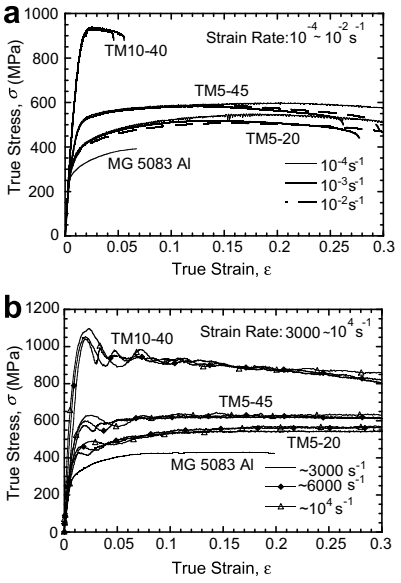

Figure 2. Stress–strain curves of the tri-modal composites under strain rates of (a) 10^{-4}–10^{-2} s^{-1} and (b) 3000–10000 s^{-1}; the stress–strain curve of the conventional MG 5083-Al is also given. The high-strain-rate curves are obtained from compression Kolsky bar tests. The oscillation in the curves is from dispersion when waves propagate in the testing apparatus and does not represent the material property.

summary of the apparent yield strength of the composites and the MG-Al5083 is given in Table 1. All of the composites exhibit higher flow strength than the MG-Al5083, and among them, the composite TM10-40 has the highest strength (928 MPa) and TM5-20 the lowest (385 MPa). TM5-20 and TM5-45 exhibit failure strains of ~0.3. The increase of B_4C volume fraction from TM5-45 to TM10-40 significantly increases the overall strength from 516 to 928 MPa, but the failure strain decreases dramatically from ~0.25 to ~0.05. TM5-20 and TM5-45 exhibit some strain hardening for strains less than 0.1, like the conventional 5083-Al; while the composite TM10-40 shows only softening after the apparent yielding. The strain hardening exponents $N = \log\sigma/\log\varepsilon$ of these composites at the strain rate of 10^{-4} s^{-1}(given in Table 1) show a decreasing trend in the order of MG-Al5083, TM5-20, and TM5-45. Strain hardening behavior is affected by damage evolution in metal matrix composites [1]. In these tri-modal composites, it is likely that the damage is mainly associated with NC Al and B_4C particles. TM5-20 appears a negative rate-sensitivity at these low strain rates, which is a manifestation of dynamic strain aging (DSA) in solution hardened aluminum alloys [12], while TM5-45 and TM10-40 do not exhibit obvious rate-dependence at these rates.

Table 1. Material properties

Composite	Theoretical density (g/cm^3)	Elastic modulus[a] (GPa)	Yield strength (MPa)	N	$\dot{\varepsilon}_0$ (s^{-1})	m
MG 5083-Al	2.70	70	273	0.18	–	–
TM5-20	2.69	90	385	0.13	2.61×10^7	0.31
TM5-45	2.69	90	516	0.05	2.61×10^7	0.31
TM10-40	2.68	110	928	–	–	–

[a] Calculated from the rule of mixture theory [15].

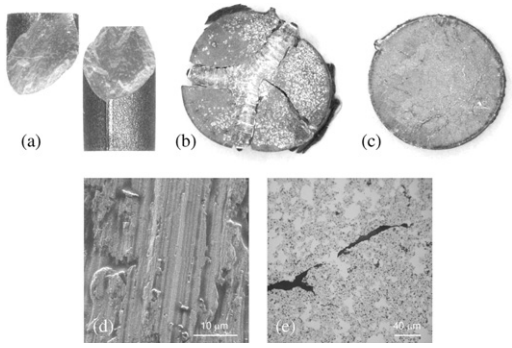

Figure 3. Deformation and failure of TM10-40 specimens after (a) quasistatic loading; dynamic loading at strain rate of (b) 3000 s^{-1} and (c) 10^5 s^{-1}; (d) SEM micrograph showing the fracture surface of (a); (e) Optical micrograph showing micro-cracks of (c). In (e), two micro-cracks have initiated and developed in the brittle phase of NC Al and B_4C (gray region with dark spots) and were stopped by MG Al (light phase).

In quasistatic tests, all specimens failed in shear with a single flat surface oriented at an angle approximately 45 degrees to the compression axis (Fig. 3a). A micrograph showing the fracture surface of TM10-40 is given in Figure 3d, where the significant shear of the material is evident. Such shear failure has not been observed in conventional Al5083 and indicates a relative brittle feature of these tri-modal composites. However, compared to composites containing only NC Al5083 and B_4C particles that fail barely in the elastic region [5], the tri-modal composites show an improved and controllable ductility as a result of the adding of the MG phase.

Figure 2b shows true stress–strain curves of TM5-20, TM5-45, and TM10-40 composites at strain rates of about 3000, 6000, and 10^4 s^{-1}. Under high-strain-rate loading, these composites exhibit similar strengths as those observed under quasistatic loading. However, the flow behaviors are markedly different from those under quasistatic loading, especially for TM10-40. Failure strains (not shown in Fig. 2b) larger than 0.2 are observed in high strain rate compression tests compared to those of 0.05 in quasistatic compression tests.

Figure 3b and c show specimens of the composite TM10-40 after compression test at strain rates of about 3000 s^{-1} and $\sim 10^4$ s^{-1}, respectively [13]. In the former one, several major cracks were developed and oriented $\sim$45 degrees to the compression axis. These major cracks result in the final failure of the specimen. The failure strain is measured from the intact circular profile of one side of the specimen (reverse side of that shown in Fig. 3b) and is $\sim$0.31, much higher than that observed in the quasistatic test. Interestingly, the test at 10^4 s^{-1} does not show any major crack, even though it experienced a much larger total strain ($\sim$0.56). Instead, a large number of micro-cracks are apparent on the specimen surface. A rate-dependent damage process in these tri-modal composites is therefore indicated: under low strain rate deformation, single or several major cracks develop to catastrophic failure of the specimen; under high strain rate deformation, micro-cracks develop and unload their neighborhood independently with less time to fully communicate with each other so as to delay or suppress the catastrophic failure of the specimen. In this composite system, the MG Al is the most ductile phase and plays significant role in this mechanism to work as cushion between the brittle regions of mixed NG Al and B_4C particles and mitigate the effects of damaging. Under high rate of loading, numerous micro-cracks nucleate in broad regions containing NG Al and B_4C particles. These micro-cracks are likely to be stopped or arrested by the intensified plastic deformation in MG Al. Some evidence of this mechanism can be found in Figure 3e, where an optical micrograph of cracks in a TM10-40 specimen after dynamic test is presented. Two micro-cracks, mostly residing in the mixing phase of NC Al and B_4C, are clearly stopped at the MG Al phase.

Shear localization is found to be the main failure mode of this composite under high strain rate loading through high-speed photography. A stress–strain curve of a rectangular TM10-40 specimen loaded under high strain rate of 4000 s^{-1} is given in Figure 4, where the insets show snap-shots from a high-speed movie of the specimen in course of deformation. Compared to specimens with circular cross-section under same strain rate loading (Fig. 2), a smaller strain to failure of 0.18 is observed due to the geometry effect of the specimen. The inset images (a)–(e) correspond to strain levels of 0, 0.11, 0.16, 0.21, and 0.3, respectively. Inset a) shows the intact specimen before arrival of the compressive wave. The specimen experienced a homogeneous deformation until the strain corresponding to inset (c) where multiple shear bands start to develop. Accordingly, the stress–strain curve starts to drop and reaches a minimum value in a strain level corresponding to inset (e) where shear bands are apparent. Note the later increase of the stress after the stress drop in the stress-strain curve is due to the constraints from the bar ends to the failed specimen, and does not represent the real compressive property of the material.

The influence of strain rate on the material behavior is shown in Figure 5. In this figure, the DSA of the composite TM5-20 and the rate-insensitivity of the composites TM5-45 and TM10-40 in the quasistatic strain rate range are obvious. Two trends in the rate-sensitivity of these composites are clear in the high strain rate region. First, TM5-20 and TM5-45 exhibit apparent strain rate

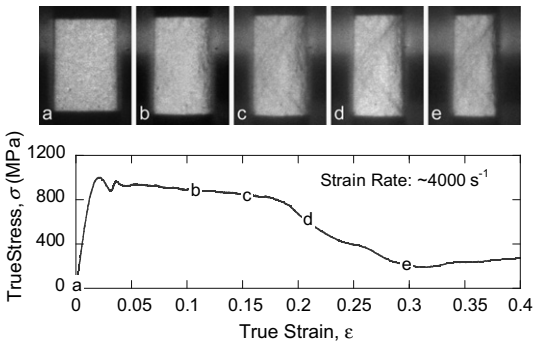

Figure 4. Stress–strain curve of a rectangular TM10-40 specimen dynamically loaded at a strain rate of $\sim$4000 s^{-1}. Insets (a)–(e) are snap-shots from high-speed photography, showing the deformation of the specimen at strain levels of 0, 0.11, 0.16, 0.21, and 0.30, respectively. Developing of multiple shear bands, starting from inset (c), contributes to failure of the specimen shown by the steep dropping of the flow stress.

hardening when strain rate increases from the quasistatic range to dynamic range. Second, TM10-40 exhibits no rate-sensitivity to this strain rate change. For metal/ceramic composites, rate-sensitivity is considered to be mainly from their ductile matrices, where dislocation motion is rate-sensitive [14]. This explains the rate-sensitivity observed in TM5-20 and TM5-45 where strain rate plays a positive effect on strength. For TM10-40, however, the development of intensive damage in brittle phases of NC Al and B_4C is significant due to the increased amount of B_4C. The effect of damage on material strength appears to counteract the dislocation effect on rate-sensitivity.

The strain rate hardening of these materials can be expressed by a modified power law $\sigma/\bar{\sigma}(\varepsilon) = 1 + (\dot{\varepsilon}/\dot{\varepsilon}_0)^m$ [14], where $\bar{\sigma}(\varepsilon)$ is a reference stress–strain function, $\dot{\varepsilon}_0$ a reference strain rate, and m is the strain rate hardening exponent. The fitted $\dot{\varepsilon}_0$ and m of TM5-20 and TM5-45, using their stress–strain behavior at the strain rate of 0.01 s^{-1} as reference, are summarized in Table 1. The strain rate hardening exponent of TM5-20 and TM5-45 is 0.31, slightly lower than the value ~0.45 of some two-phase Al/B_4C composites [14].

These tri-modal composites exhibit highly tailorable properties. The strength and the ductility of these composites can be adjusted by the B_4C and MG Al weight combinations. Adding MG Al effectively increases ductility with some sacrifice in strength, as shown in TM5-45 and TM5-20. On the other hand, increasing the amount of B_4C particles, such as from TM5-45 to TM10-40, improves strength while still maintains a minimum ductility of TM10-40. This high tailorability is mainly attributed to the tri-modal hierarchical microstructure. At high strain rates, ductility of these composites is further improved by a process of multiple micro-crack nucleation and development in the hierarchical microstructures; a uniform damaging takes place which suppresses the catastrophic localized failure that occurs in quasistatic rates. Another superior characteristic of these tri-modal composites is their light weight and, in turn, high specific stiffness and strength. The density of these composites (Table 1) is lower than most metals and composites, which gives these composites a broad prospect of applications in different environments and loading conditions.

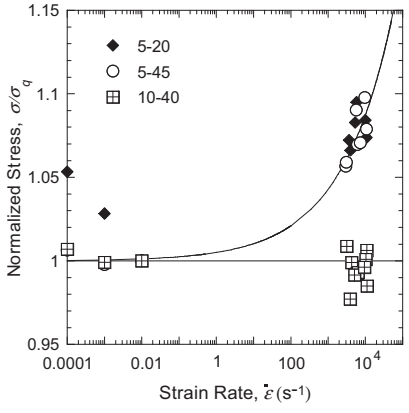

Figure 5. Strain rate-sensitivity of the tri-modal composites. Stress data are obtained at a constant strain level of 0.1 and are normalized by their corresponding quasistatic stresses at the strain rate of 0.01 s^{-1}.

In summary, three tri-modal composites, TM5-20, TM5-45, and TM10-40, which include three phases – MG 5083-Al, NC 5083-Al, and B_4C particles, have been tested under both quasistatic and high strain rates in compression. Their constitutive behavior strongly depends on their phase weight combinations. The key findings of this study are:

1) The strength of these tri-modal composites is dictated by both the amount of MG (or NC) Al and the amount of B_4C (in the reinforcing phase of NC Al and B_4C), among which the latter plays more effect on strength.
2) The hierarchical structure provides failure mitigating mechanisms to improve the material ductility; this failure mitigating mechanism is further amplified at high strain rates by a process including multiple micro-crack nucleation and development, which suppresses the catastrophic localized failure seen in quasistatic rates.
3) Shear localization is found to be the primary failure mode of these composites at both quasistatic and dynamic strain rates. One single band develops at quasistatic rates while multiple bands are able to develop at higher rates.
4) The strain rate hardening at high strain rates, provided mainly by the MG Al, is influenced by damage in the composites.

This work was performed under the auspices of the Center for Advanced Metallic and Ceramic Systems (CAMCS) at the Johns Hopkins University and supported by the United States Army Research Office through ARMAC-RTP Cooperative Agreement No. DAAD19-01-2-0003. Partial support of this work (JY and JMS) from the Office of Naval Research under Contract No. N00014-03-C-0163, is gratefully acknowledged.

[1] Y.L. Li, K.T. Ramesh, E.S.C. Chin, Acta Mater. 48 (2000) 1563.
[2] J.R. Weertman, D. Farkas, K. Hemker, H. Kung, M. Mayo, R. Mitra, H. Van Swygenhoven, MRS Bull. 24 (1999) 44.
[3] E. Ma, Scr. Mater. 49 (2003) 663.
[4] C.C. Koch, Scr. Mater. 49 (2003) 657.
[5] J.M. Schoenung, J. Ye, F. Tang, D. Witkin, Mater. Forum 29 (2005) 123.
[6] D. Witkin, Z. Lee, R. Rodriguez, S. Nutt, E. Lavernia, Scr. Mater. 49 (2003) 297.
[7] Y.M. Wang, M.W. Chen, F.H. Zhou, E. Ma, Nature 419 (2002) 912.
[8] B.Q. Han, Z. Lee, D. Witkin, S. Nutt, E.J. Lavernia, Metall. Mater. Trans. A 36 (2005) 957.
[9] J. Ye, B.Q. Han, Z. Lee, B. Ahn, S.R. Nutt, J.M. Schoenung, Scr. Mater. 53 (2005) 481.
[10] H. Kolsky, Proc. Phys. Soc. B 62 (1949) 676.
[11] R.F. Benck, E.A. Murray Jr, Tech. Report No. 2480, USA Ballistic Research Laboratories, 1975.
[12] M. Wagenhofer, M.A. Erickson-Natishan, R.W. Armstrong, F.J. Zerilli, Scr. Mater. 41 (1999) 1177.
[13] H.T. Zhang, J.C. Ye, S.P. Joshi, J.M. Schoenung, E.S.C. Chin, G.A. Gazonas, K.T. Ramesh, Adv. Eng. Mater. 9 (2007) 355.
[14] H. Zhang, K.T. Ramesh, Mater. Sci. Eng. A 384 (2004) 26.
[15] W. Voigt, Wied. Ann. 38 (1889) 573.